ELSEVIER

Spectral and thermodynamic properties of Ag(I), Au(III), Cd(II), Co(II), Fe(III), Hg(II), Mn(II), Ni(II), Pb(II), U(IV), and Zn(II) binding by methanobactin from *Methylosinus trichosporium* OB3b

Dong W. Choi [a], Young S. Do [a], Corbin J. Zea [b], Marcus T. McEllistrem [c], Sung-W. Lee [d], Jeremy D. Semrau [d], Nicola L. Pohl [b], Clint J. Kisting [a], Lori L. Scardino [c], Scott C. Hartsel [c], Eric S. Boyd [e], Gill G. Geesey [e], Theran P. Riedel [c], Peter H. Shafe [c], Kim A. Kranski [c], John R. Tritsch [c], William E. Antholine [f], Alan A. DiSpirito [a,*]

[a] *Department of Biochemistry, Biophysics and Molecular Biology, Iowa State University, Ames, IA 50011-3211, United States*
[b] *Department of Chemistry and the Plant Sciences Institute, Iowa State University, Ames, IA, 50011-3211, United States*
[c] *Department of Chemistry, University of Wisconsin-Eau Claire, Eau Claire, WI 54702, United States*
[d] *Department of Civil and Environmental Engineering, University of Michigan, Ann Arbor, MI, 48109-2125, United States*
[e] *Department of Microbiology, Montana State University, Bozeman, MT 59717, United States*
[f] *Department of Biophysics, Medical College of Wisconsin, Milwaukee, WI 53226, United States*

Abstract

Methanobactin (mb) is a novel chromopeptide that appears to function as the extracellular component of a copper acquisition system in methanotrophic bacteria. To examine this potential physiological role, and to distinguish it from iron binding siderophores, the spectral (UV–visible absorption, circular dichroism, fluorescence, and X-ray photoelectron) and thermodynamic properties of metal binding by mb were examined. In the absence of Cu(II) or Cu(I), mb will bind Ag(I), Au(III), Co(II), Cd(II), Fe(III), Hg(II), Mn(II), Ni(II), Pb(II), U(VI), or Zn(II), but not Ba(II), Ca(II), La(II), Mg(II), and Sr(II). The results suggest metals such as Ag(I), Au(III), Hg(II), Pb(II) and possibly U(VI) are bound by a mechanism similar to Cu, whereas the coordination of Co(II), Cd(II), Fe(III), Mn(II), Ni(II) and Zn(II) by mb differs from Cu(II). Consistent with its role as a copper-binding compound or chalkophore, the binding constants of all the metals examined were less than those observed with Cu(II) and copper displaced other metals except Ag(I) and Au(III) bound to mb. However, the binding of different metals by mb suggests that methanotrophic activity also may play a role in either the solubilization or immobilization of many metals *in situ*.
© 2006 Elsevier Inc. All rights reserved.

Keywords: Chalkophore; Copper-binding compound; Methanobactin; Membrane-associated methane monooxygenase; Methanotroph; *Methylosinus trichosporium* OB3b; Siderophore

* Corresponding author. Tel.: +1 515 294 2944; fax: +1 515 294 0453.
  E-mail addresses: dwon@iastate.edu (D.W. Choi), youngsdo@yahoo.com (Y.S. Do), czea@gvc.edu (C.J. Zea), mcellimt@uwec.edu (M.T. McEllistrem), sungwlz@umich.edu (Sung-W. Lee), jsemrau@engin.umich.edu (J.D. Semrau), npohl@iastate.edu (N.L. Pohl), celeeto78@yahoo.com (C.J. Kisting), scardill@uwec.edu (L.L. Scardino), hartsesc@uwec.edu (S.C. Hartsel), eboyd@montana.edu (E.S. Boyd), gill_g@erc.montana.edu (G.G. Geesey), riedeltp@uwec.edu (T.P. Riedel), shafeph@uwec.edu (P.H. Shafe), kranskk@uwec.edu (K.A. Kranski), triscjr@uwec.edu (J.R. Tritsch), wantholi@mcw.edu (W.E. Antholine), aland@iastate.edu (A.A. DiSpirito).

1. Introduction

Methanobactin (mb) is a low molecular mass (1154 Da) chromopeptide observed in both the extracellular and membrane fraction in many if not all aerobic methanotrophs [1–5]. When isolated from the membrane fraction, mb contains one copper atom and is predominately associated with the membrane-associated or particulate methane monooxygenase [5–7]. In the extracellular fraction, the majority of mb is metal free [2,5], and appears to be the extracellular component of a copper acquisition system similar to bacterial siderophore-based iron acquisition systems [2–6,8–12]. This proposed copper-siderophore, or chalkophore role [3], is based on copper uptake and localization studies [2,4–7,11], chelation of copper in soil systems [11], characterization of constitutive soluble methane monooxygenase mutants in *Ms. trichosporium* OB3b [2,4,9,12], and copper-binding studies [2,5,6,8,10].

The structure of copper containing mb (Cu–mb) following exposure to high copper concentrations showed the molecule bound one copper atom in a novel S, and N coordination by the 4-thiocarbonyl-5-hydroxy imidazolate (THI) and 4-hydroxy-5-thiocarbonyl imidazolate (HTI) moieties [3]. However, spectral, kinetic and thermodynamic studies indicate that initial coordination of Cu(II) and Cu(I) differs from the coordination observed in the crystal structure [8]. Mb appears to initially coordinate Cu(II) as tetramer or oligomer by THI and possibly Tyr (Fig. 1).

This initial coordination is followed by a reduction of Cu(II) to Cu(I), and then followed by a change in metal ligation resulting in coordination by both THI and the HTI. At Cu(II) to mb ratios above 0.25 the Cu(II) is coordinated as a dimer, followed by coordination as a monomer at Cu(II) to mb ratios above 0.5 Cu per mb (Fig. 1).

The structural similarities of mb to siderophores in the pyoverdin class [13–16] suggested that mb may prove to be a siderophore with a capacity to bind Cu(II) as well as Fe(III). Several other observations suggest mb may be involved in the mobilization of non-cuprous metals. The coupled increase in iron uptake with increased copper uptake, or copper-induced iron uptake, suggest that mb may be involved in iron uptake [5,17]. Given that mb is the major if not sole extracellular metal binding compound produced by *Ms. trichosporium* OB3b [2,6,8,10], the observation by Jenkins et al. [18] that this bacterium mobilizes Cd(II) in soil columns suggest mb may bind Cd(II). To determine if mb can function as a siderophore and/or to mobilize metals other than copper, the metal binding properties of mb were examined. In this report the initial spectral and thermodynamic properties of Ag(I), Au(III), Co(II), Cd(II), Fe(III), Hg(II), Mn(II), Ni(II), Pb(II), U(VI) and Zn(II) binding were examined with special attention given to metals which are coordinated and reduced via a mechanism similar to copper, i.e., Ag(I), Au(III), Hg(II), and Pb(II). The results show that mb is primarily involved copper mobilization, but the binding
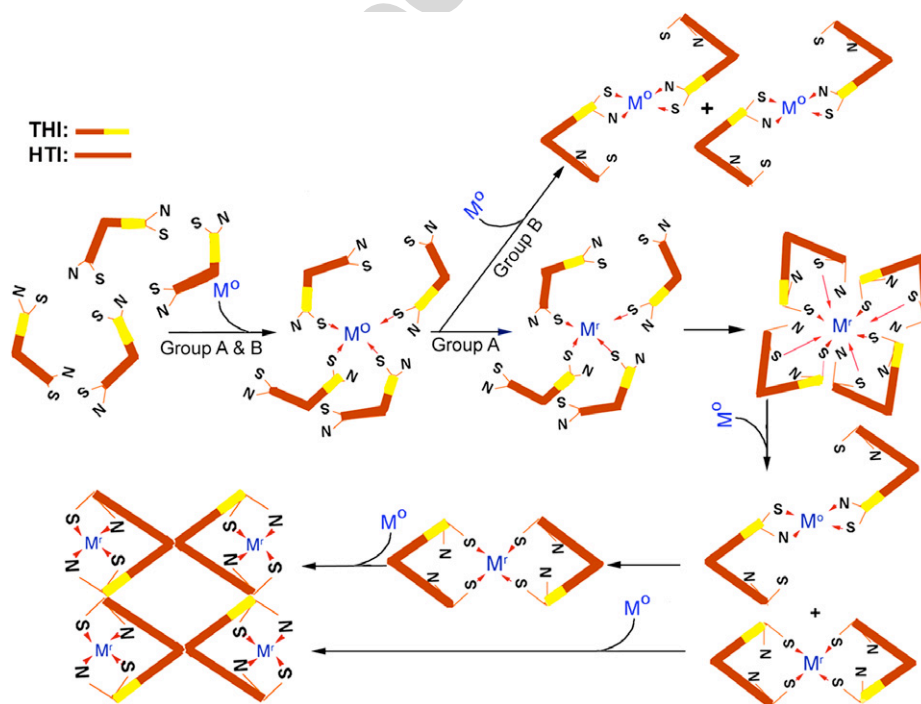
Fig. 1. Model for the binding of group A (Ag(I), Au(III), Cu(II), Hg(II), Pb(II) and U(VI)) and group B (Cd(II), Co(II), Fe(III), Ni(II), and Zn(II)) metals by mb. Mb is represented as two bars ending in the N^ε atom of each imidazolate and the S atom from the thiocarbonyl group on 4-thiocarbonyl-5-hydroxy imidazolate (THI; yellow and orange bar) and on 4-hydroxy-5-thiocarbonyl imidazolate (HTI; orange bar). Abbreviations: M^o, metal in the oxidation state added to mb solutions, and M^r, metal reduced by mb. (For interpretation of the references in colour in this figure caption, the reader is referred to the web version of this article.)

of different metals by mb suggests that methanotrophic activity also may play a role in solubilization of many metals *in situ*.

2. Experimental

2.1. Organisms culture conditions and isolation of mb

Ms. trichosporium OB3b was cultured in either 0 or 0.2 μM CuSO$_4$ amended nitrate minimal salts (NMS) medium as previously described [6]. Mb was prepared from *Ms. trichosporium* OB3b as described previously [6,8], except the rotary evaporation treatment was removed from the isolation procedure. Instead the methanol was removed during lyophilization. For preparations of metal saturated mb samples, CdCl$_2$, CoCl$_2$, FeCl$_3$, MgCl$_2$, MnCl$_2$, NiCl$_2$, or ZnSO$_4$ was added to the spent media to a final concentration of 2 mM followed by 8 h incubation in the dark at 4 °C. The spent medium was then centrifuged twice at 15,000*g* for 20 min to remove metal precipitations and loaded on a 7 × 20 cm Dianion HP-20 column (Supelco, Bellefonte, PA). Bound metal-mb were washed with four column volumes of H$_2$O and eluted with 60% methanol: 40% H$_2$O and lyophilized. Due to precipitation or altered column binding properties following exposure to excess metal concentrations, the concentration of Au(III), Fe(III), Hg(II), and U(IV) bound by mb were determined via titration experiments (see below).

2.2. Metal titrations

Metal titration experiments were determined by addition of 100 μM, 1 mM, or 10 mM solutions of AgNO$_3$, HAuCl$_4$, CdCl$_2$, CoCl$_2$, CrO$_3$, CuSO$_4$, FeCl$_3$, HgCl$_2$, MgCl$_2$, MnCl$_2$, NiCl$_2$, Pb(NO$_3$)$_2$, UO$_2$(NO$_3$)$_2$, or ZnSO$_4$ to 50 μM mb dissolved in H$_2$O, pH 6.8 as previously described for Cu(II) or Cu(I) titrations [8] unless otherwise stated. Glassware was soaked in 0.1 N HNO$_3$ for 12 h then rinsed with milliQ H$_2$O. For the metal replacement experiments, 50 μM aqueous mb solutions were preloaded with equimolar of AgNO$_3$, HAuCl$_4$, CaCl$_2$, CdCl$_2$, CoCl$_2$, CrO$_3$, CuSO$_4$, FeCl$_3$, HgCl$_2$, MgCl$_2$, MnCl$_2$, NiCl$_2$, Pb(NO$_3$)$_2$, UO$_2$(NO$_3$)$_2$, or ZnSO$_4$, incubated for a 10 min followed by the addition of equimolar CuSO$_4$ then monitored via UV–visible absorption spectroscopy every 30 s for 0.5–120 min. Between scans the samples were stored in the dark to avoid photodegradation [6].

2.3. Spectroscopy, isothermal titration calorimetry (ITC), and metal determinations

UV–visible absorption spectra, fluorescence spectra, and metal determinations via inductively coupled plasma atomic emission-mass spectroscopy (ICP-MS) were determined as previously described [7,8]. In contrast to a previous report [8], the base line was used as a reference point instead of the isosbestic points in UV–visible absorption spectra for the comparison of Δεs.

CD spectra measurements were carried out on either a JASCO J-710 spectropolarimeter (Jasco Co, Tokyo, Japan) or on a Applied Photophysics SX.18MV CD spectrophotometer as previously described [8]. Metals were titrated into 100 μM aqueous mb solution.

EPR samples were prepared by adding equimolar metals to 5 mM mb aqueous solutions. After 5 min of incubation, samples were transferred to quartz EPR tubes, then frozen in a liquid nitrogen bath, and the spectra determined as previously described [8].

ITC was performed with following modifications from the previously described procedure [8]. First, concentrations of the titrant and cell solutions were raised to 3.2 mM and 0.4 mM, respectively. Second, the interval between titrant injections were decreased to 600 s and the stirring rate decreased to 380 rpm.

2.4. X-ray photoelectron spectroscopy (XPS)

XPS was preformed on a model Phoibos-150 hemispherical analyzer (SPECS Scientific Instruments, Sarasota, FL) or on a model 5600ci spectrophotometer (Perkin–Elmer Inc., Eden Prairie, MN) as previously described [8].

2.5. Transmission electron microscopy

Gold nanoparticle production was determined by addition of 10 mM aqueous solutions of HAuCl$_4$ to 1 or 5 mM aqueous mb solutions. Mb solutions were prepared freshly and immediately dispensed into 1.8 ml glass vials. Gold solutions were added to the glass vials containing mb solutions with a final molar ratios of 0, 0.1, 0.2, 0.4, 0.75, 1.0, 1.5, 2.0, 3.0, 4.0, 5.0, 10.0, 15.0, or 20.0 Au(III) to mb. All samples were incubated for 15 min with or without stirring. In some cases the Au–mb solutions were spotted on formvar-coated Ni or Cu grids. Other samples were subjected to one freeze thaw cycle before spotting on formvar-coated Ni or Cu grids. Lastly some samples were centrifuged at 10,000*g* for 2 min at room temperature and the loose red pellet spotted on formvar-coated Ni grids. The samples on Ni or Cu grids were then dried under vacuum and examined with a JEOL 1200X scanning/transmission electron microscope.

3. Results and discussion

3.1. Metals bound by mb and metals binding groups

Initial screening by UV–visible absorption spectroscopy showed that in the absence of Cu(II) or Cu(I), mb will bind Ag(I), Au(III), Cd(II), Co(II), Fe(III), Hg(II), Mn(II), Ni(II), Pb(II), U(VI), or Zn(II) but not Ba(II), Cr(VI), La(III), Mg(II), or Sr(II) (see below). Based on the redox and spectral properties described below, the metals bound by mb were placed into two groups. Choi et al. [8] recently

described the spectral and thermodynamic properties of Cu(II) and Cu(I) which are designated in mb group A metals. Metals that showed a final coordination via 4-thiocarbonyl-5-hydroxy imidazolate (THI), 4-hydroxy-5-thiocarbonyl imidazolate (HTI) and possibly Tyr were placed in group A. In general, mb also reduced these metals without the addition of an external reductant. Lastly, depending on the metal concentration, mb coordinated group A metals as either a tetramer, dimer, or monomer. In addition to Cu, Group A metals include Ag(I) and Au(III), Hg(II), Pb(II) and possibly U(VI).

Group B metals consist of the transition metals Cd(II), Co(II) Fe(III), Mn(II), Ni(II), and Zn(II). Group B metals were characterized by a final coordination to THI and without a change in the oxidation state of the metal. In addition, depending on the concentration of group B metal, mb coordinated group B metals as either a tetramer or dimer, but not as a monomer. Thus, even in the presence of excess metals, mb coordinates group B metals as a dimer. With respect to the copper-binding model proposed by Choi et al. [8], coordination of group B metals stops after the initial two binding steps (Fig. 1).

3.2. UV–visible absorption spectra

3.2.1. Group A metals

As observed with copper [8], the binding of Au(III) (Fig. 2A and B), Ag(I) (Fig. 3A and B) and U(VI) (results not shown) resulted in a decreased absorption at 394 nm suggesting coordination to THI (Table 1). In addition to a decrease in absorption at 394 nm, the addition of Hg(II) or Pb(II) also resulted in a shift in the absorption maxima to 385 and 400 nm, respectively (results not shown). Spectral changes were also observed at 340 nm following the addition of group A suggesting coordination to HTI. However, in contrast to Cu(I), Cu(II) and U(VI) which showed
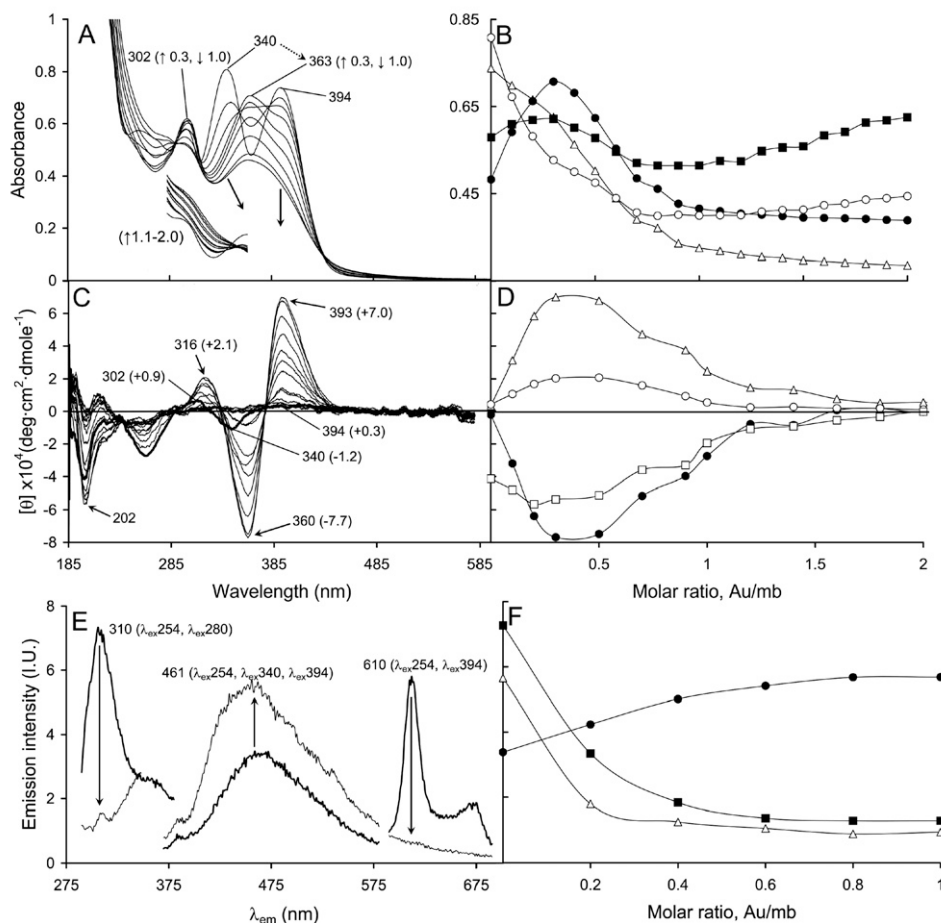

Fig. 2. (A) UV–visible absorption spectra of mb following addition of 0.1, 0.2, 0.3, 0.4, 0.6, 0.8.1.0, 1.2, 1.4, 1.6. 1.8 and 2.0 Au(III) per mb. Arrows indicate the direction of spectra changes upon Au(III) additions. (B) Absorption changes at 394 ($\triangle$), 363 ($\bullet$), 340 ($\circ$), and 302 ($\blacksquare$) following 0.1 to 2.0 Au(III) additions. Due to the development of strong absorption/light scattering below 300 nm with 1.1 to 2.0 Au(III) additions, absorption changes in this region could not be monitored (shown in insertion in panel A). (C) CD spectra of mb as isolated (thick line) and following additions of 0.1 to 2.0 molar equivalents of Au(III) (thin lines). (D) The effect of Au(III) addition on the CD spectra at 393 ($\triangle$), 360 ($\bullet$), 316 ($\circ$), and 202 nm ($\square$). (E) Emission spectra of mb in aqueous solution with different excitation wavelength (nm). λ_{ex} = 280, 340, and 394 nm at ambient temperature (thick lines). Arrows indicate the direction of spectrum changes upon Au(III) additions and thin lines show the spectra upon completion of changes. (F) Emission intensity changes at 610 (λ_{ex} = 394 nm, $\triangle$), 461 (λ_{ex} = 340 nm, $\bullet$), and 310 nm (λ_{ex} = 280 nm, $\blacksquare$).
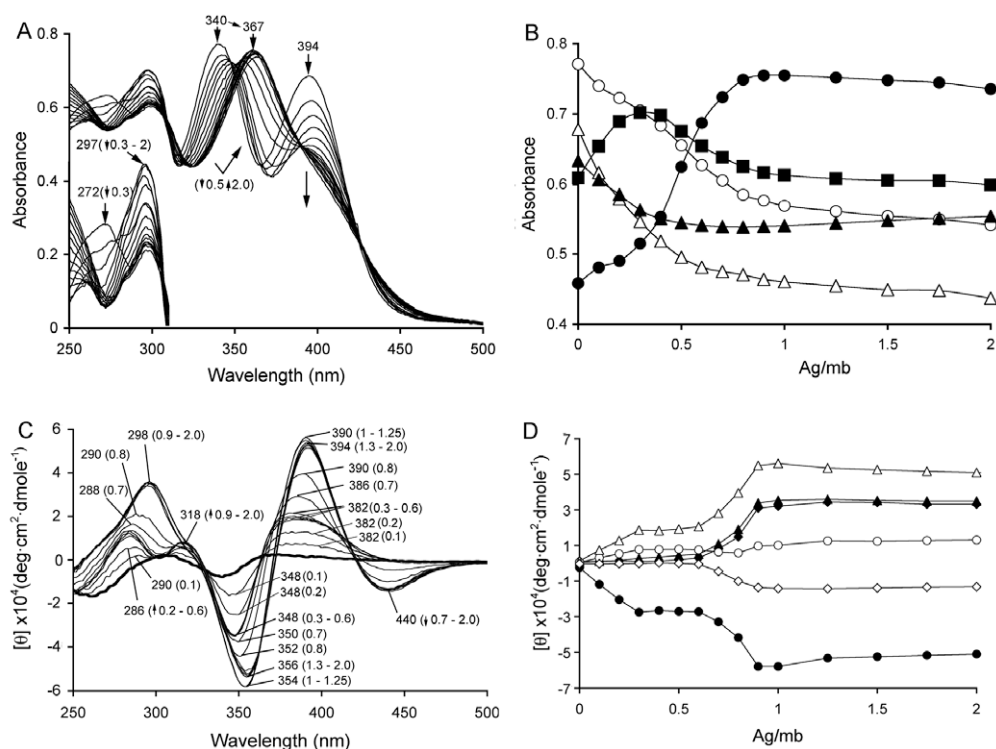
Fig. 3. (A) UV–visible absorption spectra of mb following addition of 0.1, 0.2, 0.3, 0.4, 0.6, 0.8.1.0, 1.25, 1.4, 1.6. 1.8 and 2.0 Ag(I) per mb. Arrows indicate the direction of spectra changes upon Ag(I) additions. (B) Absorption changes at 394 ($\triangle$), 363 ($\bullet$), 340 ($\circ$), 302 ($\blacksquare$), 272 ($\blacktriangle$) nm following 0.1 to 2.0 Ag(I) additions. (C) CD spectra of mb as isolated (thick line) and following additions of 0.1 to 2.0 molar equivalents of Ag(I) (thin lines). (D) The effect of Ag(I) addition on the CD spectra at 404 ($\diamond$), 390 ($\triangle$), 354 ($\bullet$), 314 ($\circ$), and 300 ($\blacklozenge$) 283 ($\blacksquare$) nm.

Table 1
Molar absorption coefficients (ε) of mb and metal-mb

Proteins	$\varepsilon_{340}(mM^{-1}\,cm^{-1})$	$\Delta\varepsilon_{340}(mM^{-1}\,cm^{-1})$	$\varepsilon_{394}(mM^{-1}\,cm^{-1})$	$\Delta\varepsilon_{394}(mM^{-1}\,cm^{-1})$
mb	18.24	–	16.07	–
Group A				
Cu–mb	13.55	4.69	9.75	6.31
Au–mb	9.01	9.23	7.07	9.00
Hg–mb	11.57	6.67	12.92	3.14
U–mb	16.24	2.00	13.98	2.09
Group B				
Cd–mb	18.73	−0.49[a]	11.33	4.74
Co–mb	18.60	−0.36[a]	12.78	3.29
Fe–mb	18.17	0.07	10.19	5.88
Mn–mb	20.54	−2.30[a]	11.28	4.79
Ni–mb	17.88	0.36	12.21	3.86
Zn–mb	19.69	−1.45[a]	11.13	4.94

[a] An increase in absorbance was observed.

a decreased absorbance at 340 nm following metal binding [8], the spectral changes associated with HTI following the addition of other group A metals were complex. At Au(III) or Hg(II) concentrations ⩽0.3 metal per mb, a red shift in the absorption maximum from 340 to 363 nm was observed with an increased absorption at 363 nm (Fig. 2A and B). At Au(III) or Hg(II) concentrations >0.3 metal per mb, a decrease in absorbance at 363 nm was observed. A similar response to metal concentration was observed at 302 nm, where an increase in absorbance occurred at low metal concentrations (i.e., ⩽0.3 metal per mb) followed by a decreased absorbance at metal to mb ratios between 0.3 and 1.0 metal per mb and an increased absorbance at metal to mb concentrations above 1.0. The spectral changes associated with Hg(II) were identical to Au(III) (results not shown).

The spectral changes at 302 nm following the addition of Ag(I) were identical to Au(III) with an initial increase a Ag(I) to mb ratios ⩽0.3 Ag(I) per mb, followed by a decrease at higher Ag(I) to mb ratios. The spectral shifts

at 340 nm following the addition of Ag(I) were also similar to Au(III) and Hg(II) with a red shift to 367 nm, however, the changes in absorption were opposite to that observed with Au(III), with an initial decrease in absorption from HTI nm at Ag(I) concentrations $\leqslant 0.3$ Ag(I) per mb followed by an increased absorption at higher Ag(I) concentration (Fig. 3A and B). The spectral changes associated with HTI following the addition of Pb(II) resulted in a decrease in absorption along with a spectral shift to 350 nm (results not shown). The results suggest coordination to HTI for all group A metals, but the coordination may differ between members of the group A metals and that the interactions between metal and HTI may change at different metal to mb ratios.

3.2.2. Group B metals

The binding of group B metals by mb resulted in a decreased absorption at 394 nm, with either no change (Ni and Fe), or an increased in absorption at 340 nm (Cd, Co, and Zn) (Fig. 4; Table 1). In the case of Mn(II), a blue shift in the maxima of at 394 nm to 377 nm following metal addition was also observed (results not shown). In addition, with the exception of Ni(II) and Mn(II), little to no changes in absorbance were observed in the 250–310 nm range for this metal group. Mn(II) addition resulted in a decrease in absorption at 302 nm without an associated increase in absorption at 282 nm. The absence of an absorbance change at 282 nm with decreased absorption at 302 nm suggests the absorption maxima at 282 and 302 nm do not represent the phenolic and phenoxide ion forms of Tyr and may represent a charge transfer band [8,19].

The final spectral changes associated with the binding of group B metals were similar to those observed in the initial coordination to Cu(II) suggesting these metals were bound as a dimer via the THI moieties (Fig. 1) [8]. To determine if
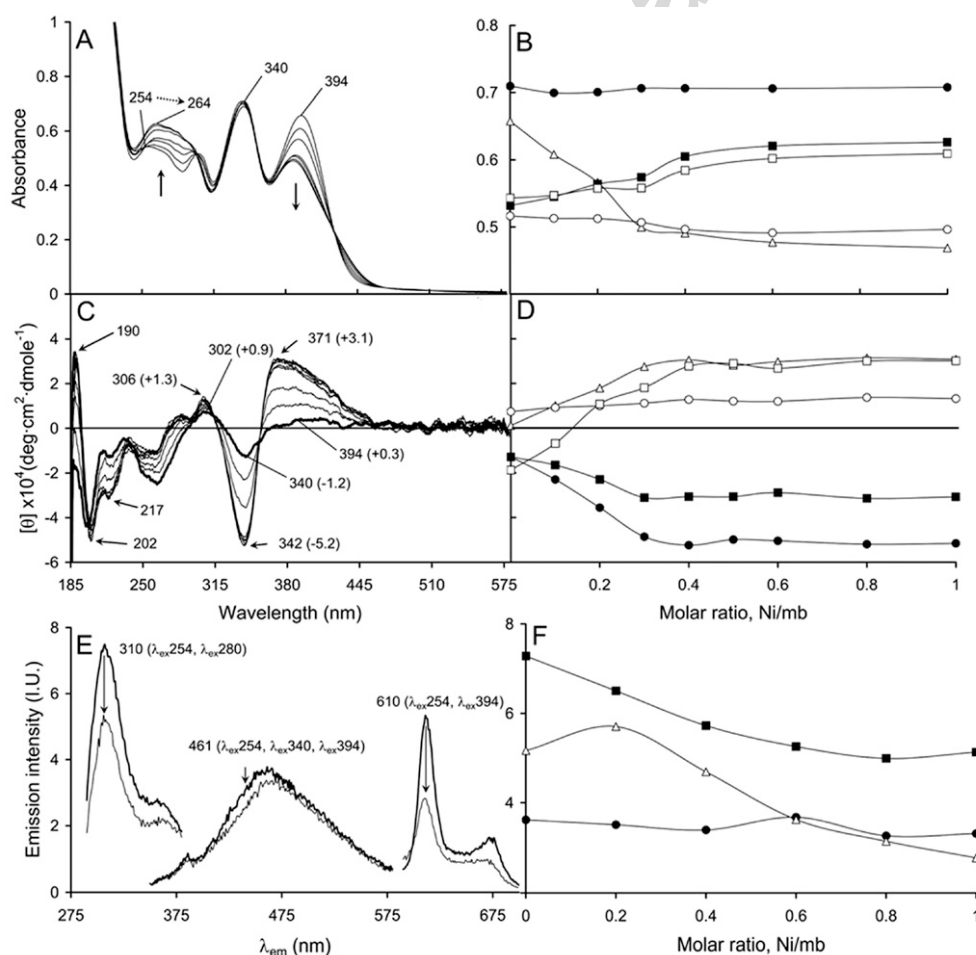

Fig. 4. (A) UV–visible absorption spectra of mb following addition of 0.1, 0.2, 0.3, 0.4, 0.6, 0.8 and 1.0 Ni(II) per mb. Arrows indicate the direction of spectra changes upon Ni(II) additions. (B) Absorption changes at 394 ($\triangle$), 340 ($\bullet$), 302 ($\circ$), 264 ($\blacksquare$), and 254 nm ($\square$) following Ni(II) additions. (C) CD spectra of mb as isolated (thick line) and following additions of 0.1 to 1.0 molar equivalents of Ni(II) (thin lines). (D) The effect of Ni(II) addition on the CD spectra at 371 ($\triangle$), 342 ($\bullet$), 306 ($\circ$), 217 ($\blacksquare$), and 190 nm ($\square$). (E) Emission spectra of mb in aqueous solution with different excitation wavelength (nm). $\lambda_{ex} = 280$, 340, and 394 nm at ambient temperature (thick lines). Arrows indicate the direction of spectrum changes upon Ni(II) additions and thin lines show the spectra upon completion of changes. (F) Emission intensity changes at 610 ($\lambda_{ex} = 394$ nm, $\triangle$), 461 ($\lambda_{ex} = 340$ nm, $\bullet$), and 310 nm ($\lambda_{ex} = 280$ nm, $\blacksquare$).

Table 2
Molar ratios of Cu(II) and group B metals per mb

Metal	mb	Cu–mb	Cd–mb	Zn–mb	Ni–mb	Mn–mb	Co–mb
Cu(II)	0.0376	1.552	bd	0.0014	0.0010	0.0002	bd
Cd(II)	0.003	0.0006	0.6079	bd	bd	bd	0.0008
Zn(II)	0.001	bd[a]	bd	0.6575	0.0017	0.0040	bd
Ni(II)	0.0001	0.0029	0.0005	0.0002	0.7603	0.0004	0.0107
Mn(II)	0.0004	bd	bd	0.0028	0.0014	0.6778	0.0003
Co(II)	0.0003	0.0016	0.0017	0.0004	0.0002	0.0001	0.8068

Mb was treated with an saturating concentrations of (50 fold molar excess) of Cu(II) (Cu–mb), Cd(II) (Cd–mb), Zn(II) (Zn–mb), Ni(II) (Ni–mb), Mn(II) (Mn–mb), or Co(II) (Co–mb), collected on a Dianion HP-20 column, washed with five column volumes of H_2O, then eluted and freeze dried. Standard variance was equal to or less than 20%.
[a] Below detection.

the final coordination of group B metals was a dimer, the concentration of metal associated with mb were determined following exposure to excess metal concentrations. Consistent with the UV–visible absorption titrations, the concentration of Cd(II), Co(II), Mn(II), Ni(II), or Zn(II) bound to mb was approximately half of that observed with Cu(II) demonstrating mb binds these metals as a dimer even in the presses of saturating metal concentrations (Table 2).

3.3. Fluorescence spectroscopy

As observed with Cu, [8], the addition of other group A, and with the exception of Mn(II), group B metals quenched emissions from THI following excitation at 394 nm (λ_{ex394}) (Figs. 2E and F, 3E and F; Table 3). The addition of Mn(II) had no effect on emission from THI (results not shown). With the exception of Co(II) and Mn(II), the addition of group A and B metals also quenched emission from

Table 3
Change in emission intensities from Tyr, following excitation at 280 nm (λ_{ex280}), THI following excitation at 394 nm (λ_{ex394}), and HTI following excitation at 340 nm (λ_{ex340}) following the addition of equimolar concentrations of metals to mb

Metal	Change in emission intensity		
	Tyr	HTI	THI
	310 nm	461 nm	610 nm
Group A			
Cu(II)[a]	−4.88[b]	−0.03[b,d]	−3.82[b]
	−1.00[c]	−0.83[c]	−1.57[c]
Hg(II)	−4.26	+1.11	−3.82
Au(III)	−6.36	+2.01	−3.80
Group B			
Cd(II)	−0.43	+1.76	−1.72
Co(II)	−0.10	−0.43	−1.72
Fe(III)	−4.84	−0.92	−3.23
Ni(II)	−2.85	−0.37	−2.70
Zn(II)	−0.88	+0.52	−4.0
Mn(II)	+0.17	−0.44	+0.37

[a] From Choi et al. [8].
[b] As isolated by Choi et al. [8].
[c] Isolated following Cu(II) saturation and Na₂EDTA treatment [8,10].
[d] *Note*: Absence of quenching resulted from the reduction of Cu(II) to Cu(I) before coordination to HTI [8].

Tyr suggesting Tyr was either involved in metal coordination or was proximal to the metal coordination site (Figs. 2E and F, 3E and F; Table 3).

The addition of groups A and B metals had mixed effects on emission from HTI following excitation at 340 nm (Fig. 3E and F). The addition of Cd(II), Zn(II), Hg(II) and Au(III) to mb resulted in an increase in emission from HTI (Fig. 4E and F) following excitation at 254, 340, or 394 nm. In the case of Au, the emissions observed at 461 nm decreased at Au(III) to mb ratios ⩾0.8 following excitation at 254 and 340 nm with new emission maxima at 421, 441, and 524 nm following excitation at 394 nm (Fig. 5A and B). These new emission maxima were not observed with excitation at 254 or 340 nm nor were they observed with Hg(III). Cation induced fluorescence has been shown to occur with removal or separation of an internal quencher following cation binding, or via cation binding to the internal quencher [20,21]. Cation induced increased fluorescence has also been observed in chlorophyll *a* in the presence of negatively charged gold nanoparticles [22]. In this analogy gold nanoparticles functioned as an electron shuttle from an electron source such as THI to HTI. XPS spectroscopy demonstrated the reduction of Au(III) to Au(0) and examination of Au–mb complexes by transmission electron microscopy (TEM) and UV–visi-
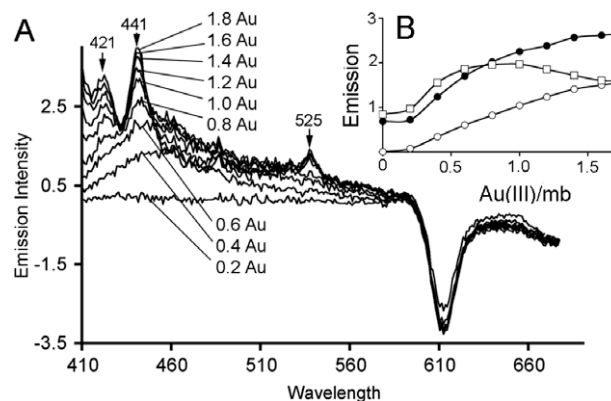

Fig. 5. A. Difference fluorescence spectra of mb following the addition of 0.2, 0.4, 0.6, 0.8, 1.0, 1.2, 1.4, 1.6, or 1.8 molar equivalences of Au(III) minus mb. B, Emission intensity changes at 461 nm (λ_{ex} = 394 nm, ○), 421 nm (λ_{ex} = 394 nm, ●), and at 441 nm (λ_{ex} = 394 nm, □).

ble absorption spectroscopy showed the formation of nanoparticles at Au to mb ratios above 1.2 Au per mb (see below).

3.4. Circular dichroism spectroscopy

The UV-CD spectrum of mb showed a strong negative band below 200 nm with negative shoulders at 202 nm and 217 nm (Figs. 2C and 4C), characteristic of an unordered polypeptide [23]. Like the UV absorption spectra, the CD spectra of the group A metals were complex and depended on the metal to mb ratio (Fig. 2). At Au(III) (Fig. 2C and D) or Hg(II) to mb concentrations ≤0.4 metal to mb, the UV-CD spectra was similar to that of Cu [8]. However, at concentrations of metal to mb >0.5, the trend reversed. The UV-CD spectra of Ag(I) was also complex with the development of an absorption maxima at 288 nm at Ag(I) to mb ratios ≤0.7 Ag(I) per mb followed by a red shift to 298 nm at Ag(I) to mb ratios between 0.7 and 0.9 Ag(I) per mb (Fig. 3C and D). At Ag(I) to mb ratios ≥0.9 nm, the absorption intensity at 298 nm does not change, but a new absorption maxima at 318 nm was observed. The absorption maxima between 286 and 318 nm may represent changes in both the environment and oxidation state of the Tyr. Addition of group B resulted in positive band enhancements at 190 nm, suggesting the development of α-helical characteristics (Fig. 4C and D).

The visible CD spectra following metal binding showed the development of an exciton coupled spectrum between the two-chromophore system (THI and HTI) with all metals tested (Figs. 2–4). The CD spectra in the 315–415 nm region following metal additions were consistent with a Cotton effect involving the THI and HTI [23–25]. At molar ratios <0.3 Au(III) or Hg(II) per mb, the visible-CD spectra were similar to that observed following copper addition (Fig. 2C and D) [8]. The CD-spectra associated with HTI following the addition of Au(III) or Ag(I) resulted in a red shift from 340 nm to 360 and 354 nm, respectively, which were similar to that observed in the UV–visible absorption spectra, with an associated negative band enhancement. The CD-spectra from THI showed a positive band enhancement with little or no shift in the absorption maxima. The absence of a shift in the absorption maxima of both THI and HTI in the CD-spectra suggest little to no change in the hydrophobicity of the environment of these groups following metal binding. In contrast to Cu [8], little change in the visible CD spectra was observed at Au(III) or Hg(II) to mb ratios between 0.3 and 0.5 (Fig. 2C and D) and between 0.3 and 0.6 Ag(I) per mb (Fig. 3C and D) suggesting little to no changes in the orientation between THI and HTI occurred in this concentration range. At Au(III) or Hg(II) concentrations >0.5 per mb, the trends throughout the visible CD-spectra reversed and with the exception of the spectral shift of HTI, the spectra at 2.0 Au(II) or Hg(II) per mb were similar to metal free mb. At Ag(I) to mb ratios >0.6, the spectral changes

were essentially opposite to that observed with Au(III) or Hg(II) (Fig. 3C and D).

In group B a negative band enhancement near 340 nm (2nd Cotton effect, HTI) and a positive band enhancement between 360 nm and 370 nm (1st Cotton effect, THI) were observed with metal addition suggesting the two chromophores were brought together with a counter-clockwise twist (positive chirality) (Fig. 4C and D) [23–25]. In contrast to Cu [8], the absorbance maxima associated with HTI following the addition of group B metals remained near 340 nm, suggesting the hydrophobicity of the environment around HTI did not change following metal binding. The absorption maxima associated with THI showed a blue shift indicating THI moved to a more hydrophobic environment following the binding of group B metals. This spectral shift was opposite to that observed with Cu suggesting the conformation changes associated with the binding of group B metals were in an opposite rotation to the changes associated with the coordination of Cu(II) or Cu(I) [8].

In contrast to copper [8], no strong relationships between Tyr and HTI were observed in the CD spectra following the addition of other group A and group B metals (Figs. 2–4).

3.5. Electron paramagnetic resonance (EPR) and X-ray photoelectron spectroscopy (XPS): oxidation state of metals bound to mb

X-band EPR spectra of Fe–mb, Co–mb (Fig. 6), and Mn–mb (not shown) samples suggest metal coordination, but not reduction by mb (Fig. 6). Ferric saturated mb samples showed a narrowing of the $g = 4.3$ peak suggesting coordination and possible cluster formation similar to that observed with a variety of siderophores (Fig. 6A) [26]. XPS-spectroscopy of Fe–mb complexes confirmed iron associated with mb remained in the ferric state, in contrast to Cu(II) which is reduced to Cu(I) [2,3,5,8]. The EPR
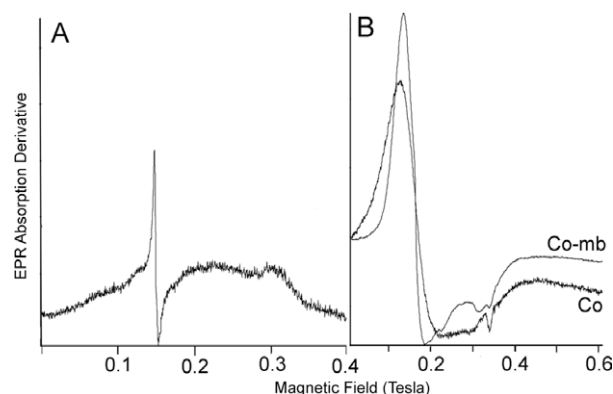

Fig. 6. X-band EPR spectra at 77 K of mb (concentration 4 mM) following the addition of Fe(III) (A), and Co(II) (B) to mb. Experimental conditions: modulation amplitude, 5 G, modulation frequency, 100 KHz, microwave power, 5 mW, temperature 77 K.

spectra of Co–mb was narrower than Co(II), again suggesting coordination without reduction (Fig. 6B). Ni–mb showed no Ni EPR signal, which was surprising considering XPS spectra showed the oxidation state Ni(II) did not change following binding to mb.

XPS showed that the group A metal, Au(III), was reduced to Au(0) by mb. Like Cu(II) more than one Au(III) were reduced per mb [8] (Fig. 7). In fact, Au(III) was not detected in reaction mixtures until the Au to mb ratio was >2 Au(III) per mb. Examination of Au–mb complexes by transmission electron microscopy (TEM) showed the Au(0) remained associated with mb even at high Au(0) to mb ratios with little to no detection of nanoparticles (Fig. 8A–C). However, if samples were centrifuged or subjected to one freeze thaw cycle nanoparticle formation was observed at Au to mb ratios above1.2 Au per mb (Fig. 9D). Following a freeze-thaw cycle or centrifugation, the nanoparticle sizes ranged from 2.5 to 30 nm, with the majority (60%) in the 11–20 nm particle range. If Au–mb solutions were examined on formvar-coated copper grids nanoparticle formation was also observed (Fig. 8E and F). Nanoparticles formed on copper grids were significantly smaller, average particle size 3.7 ± 1.1 nm, than following centrifugation or a freeze-thaw cycle. The oxidation states of Hg and Ag bound to mb were not determined, but formation of insoluble gray to black precipitates following the addi-

Fig. 8. Transmission electron micrographs of methanobactin solutions following the addition of 1 (A), 1.5 (B), or 2 (C) Au per mb, samples were dried on formvar-coated Ni grids. (D) TEM of 2 Au per mb following one freeze-thaw cycle, samples were dried on formvar-coated Ni grids. TEM of 5 (E) and 10 (F) Au per mb samples dried on formvar-coated Cu grids.

tion of Hg(II) or Ag(I) suggested these metals were also reduced by mb.

Metal free mb shows two sulfur signals, one at approximately 163.3 eV which has been assigned to Cys and Met S [8,27–29] and one at 161.4 eV [8,27–29] which has been attributed to thiocarbonyl S [8] (Fig. 9). As with the addition of Cu(II) [8], the addition of Au(III) resulted in an increased signal intensity at 163.3 eV and a binding energy shift of the thiocarbonyl S at 161.3 eV. The increased signal intensity at 163.3 eV and the binding energy shift of the thiocarbonyl S were complete at Au:mb ratios ≤0.3 Au per mb suggesting that mb initially binds Au as a tetramer. The similarity in the concentration of Cu(II) [8] and Au(III) required to complete the binding energy shift of the thiocarbonyl S was unexpected since Au(III) binding is followed by a three electron reduction and Cu(II) binding results in a one electron reduction suggesting the energy shift in the thiocarbonyl S followed metal binding and not necessary a change in oxidation state. A previous publication [8] reported the binding energy shift of the thiocarbonyl S occurred at Cu(II) to mb ratios ≤0.5. However, a more complete titration with Cu(II) has shown the binding energy shift of the thiocarbonyl S was complete at Cu(II) to mb ratios ≤0.3 Cu(II) per mb (results not shown).
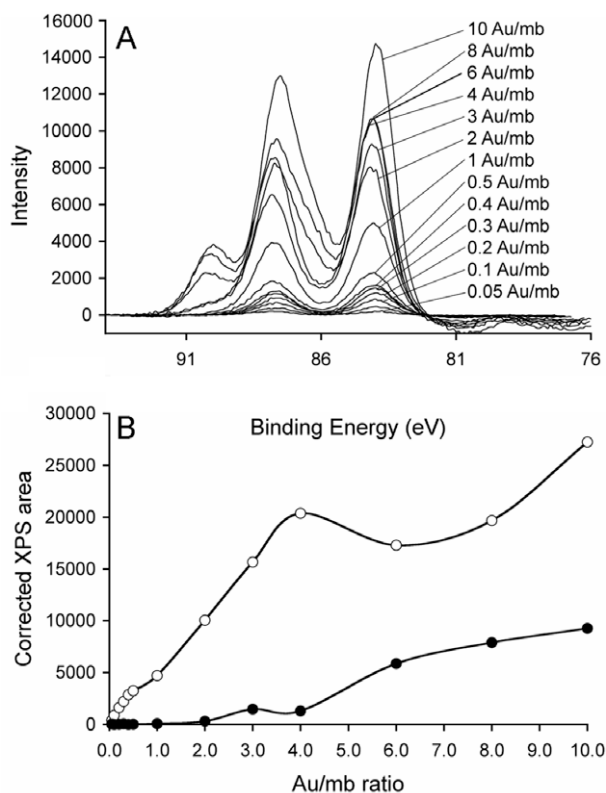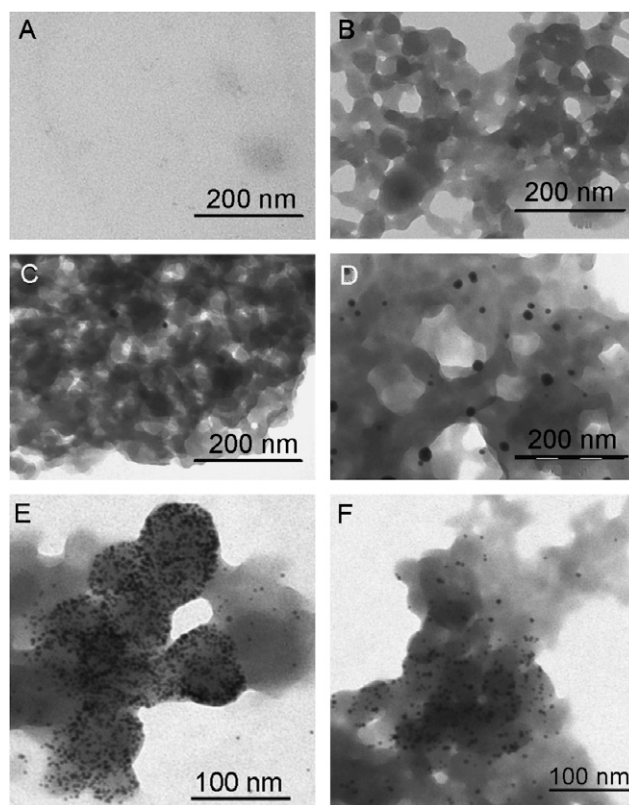

Fig. 7. (A) Gold X-ray photoelectron spectra of mb at gold to mb molar ratios between 0.05 and 10 Au per mb. (B) Corrected signal from Au(0) (○) and Au(III) (●) at different gold:mb molar ratios.
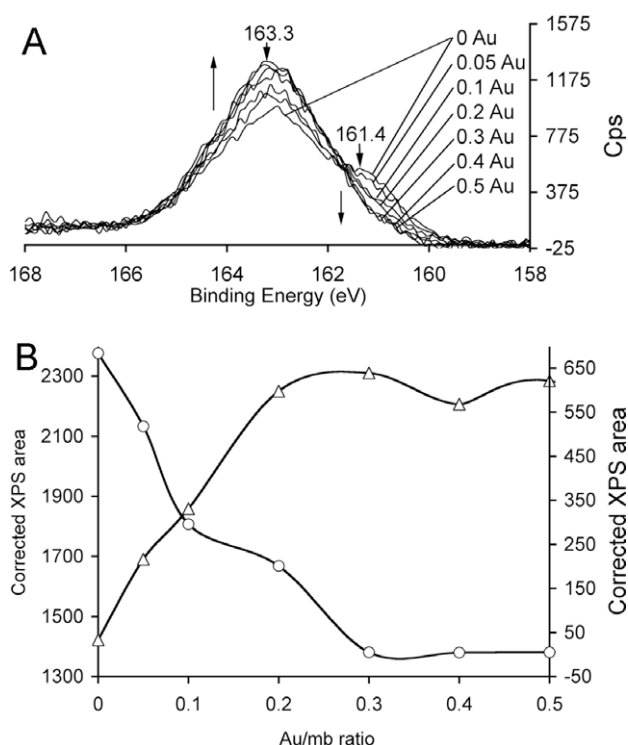
Fig. 9. (A) Sulfur XPS of mb at gold to mb molar ratios between 0.05 and 0.5 Au per mb. (B) Corrected signal from Cys and Met S (△) and thiocarbonyl S (○) at different gold:mb molar ratios. Scale on the right is for signal intensity at 163.3 eV and the scale on the left axis is for signal intensity at 161.4 eV. Arrows indicate the direction of spectrum changes upon Au(III) additions.

3.6. Isothermal titration calorimetry (ITC)

With the exception of Co(II), Pb(II) and Mn(II), all of the metals examined fit a two-site binding model better than a one-site binding model (Table 4). Most of the metals followed titration curves similar to Hg(II) (Fig. 10A), Ni(II) (Fig. 10D) or Ag(I) (Fig. 10C), with extreme transitions observed with Au(III) (Fig. 10B) and Zn(II) (Fig. 10E). The cause for the initial increase in free energy change with increased Au(III) concentration was not determined, but may be associated with the formation of Au(0) nanoparticles (Fig. 10B). The reason for the transition from exothermic to endothermic in Zn(II) titrations was not determined (Fig. 10E). The binding constants observed with non-Cu group A and group B metals were well below the binding constants observed with Cu(II) (Table 4, Fig. 10) and is consistent with its proposed role as a chalkophore [8].

3.7. Summary and concluding remarks

In contrast to iron siderophores, which are generally specific for Fe(III) [14,16,30–32], the results presented here show mb will bind a variety of metals. The binding of different metals by mb is intriguing and suggests that although mb preferentially binds copper, mb produced by methanotrophs may play a role in solubilization of many metals *in situ*. One of the persistent and substantial problems in remediation of hazardous waste sites is the

Table 4
Thermodynamic parameters as measured by ITC for metal binding to mb

Parameter	Group A				
	Cu(II)[a]	Ag(I)	Au(III)	Hg(II)	Pb(II)
N_1(metal mb^{-1})	0.11 ± 0.003	0.47 ± 0.006	0.1 ± 0.19	0.25 ± 0.005	0.61 ± 0.003
K_1(M^{-1})	$3.3 \times 10^{34} \pm 3.0 \times 10^{11}$	$2.6 \pm 0.4 \times 10^7$	$1.0 \pm 0.5 \times 10^5$	$9.9 \pm 2.9 \times 10^6$	$6.84 \pm 0.4 \times 10^5$
ΔH_1(kcal mol^{-1})	-146	$-2.0 \pm 0.2 \times 10^4$	$67 \pm 2.6 \times 10^4$	-25.1 ± 0.02	$-6.9 \pm 0.04 \times 10^3$
ΔS_1(cal mol^{-1} deg^{-1})	-331	-32.9	2.2×10^5	-52.3	3.58
ΔG_1(kcal mol^{-1})	-47.2	-10.1	1.44×10^3	-9.81	-8.0×10^3
N_1(metal mb^{-1})	0.14 ± 0.01	0.75 ± 0.007	0.38 ± 0.16	0.42 ± 0.01	–
K_1(M^{-1})	$2.6 \pm 0.5 \times 10^8$	$4.7 \pm 0.45 \times 10^4$	$1.8 \pm 0.2 \times 10^5$	$89.9 \pm 0.01 \times 10^4$	–
ΔH_1(kcal mol^{-1})	-28.1 ± 0.11	$-1.1 \pm 0.23 \times 10^4$	3.1 ± 0.7	-16.2 ± 0.05	–
ΔS_1(cal mol^{-1} deg^{-1})	-55.6	-9.53	34.5	-31.7	–
ΔG_1(kcal mol^{-1})	-11.46	-7.74	-7.18	-6.92	–
χ^2	6.47×10^4	7.14×10^4	3.9×10^5	1.76×10^5	1.27×10^4

	Group B					
	Cd(II)	Co(II)	Fe(III)	Mn(II)	Ni(II)	Zn(II)
N_1(metal mb^{-1})	0.2 ± 0.07	0.49 ± 0.003	0.27 ± 0.007	0.54 ± 0.005	0.27 ± 0.023	0.41 ± 0.004
K_1(M^{-1})	$1.3 \pm 0.8 \times 10^6$	$1.1 \pm 0.2 \times 10^6$	$9.7 \pm 0.6 \times 10^5$	$7.7 \pm 1.8 \times 10^5$	$4.9 \pm 0.9 \times 10^5$	$4.5 \pm 1.4 \times 10^6$
ΔH_1(kcal mol^{-1})	-3.15 ± 1.7	-4.08 ± 0.05	-5.31 ± 0.38	-0.07 ± 0.001	-3.15 ± 1.69	-0.32 ± 0.01
ΔS_1(cal mol^{-1} deg^{-1})	17.4	13.9	5.0	26.7	5.9	29.4
ΔG_1(kcal mol^{-1})	-8.34	-8.22	-6.80	-8.02	-7.75	-9.08
N_1(metal mb^{-1})	0.22 ± 0.01	–	0.3 ± 0.007	–	0.18 ± 0.02	0.13 ± 0.04
K_1(M^{-1})	$1.1 \pm 0.6 \times 10^7$	–	$1.7 \pm 0.7 \times 10^5$	–	$1.17 \pm 0.5 \times 10^7$	$1.8 \pm 0.1 \times 10^4$
ΔH_1(kcal mol^{-1})	-18.96 ± 1.04	–	-8.15 ± 0.08	–	-6.89 ± 0.26	2.40 ± 0.78
ΔS_1(cal mol^{-1} deg^{-1})	-31.3	–	1.14	–	9.23	27.5
ΔG_1(kcal mol^{-1})	-9.6	–	-8.49	–	-9.64	-5.8
χ^2	1.01×10^5	1.95×10^4	4.70×10^3	9.39	2.82×10^4	7.26×10^5

[a] Thermodynamic parameters for Cu(II) were taken from Choi et al. [8], for comparison purposes the third binding constant for Cu(II) was not included.
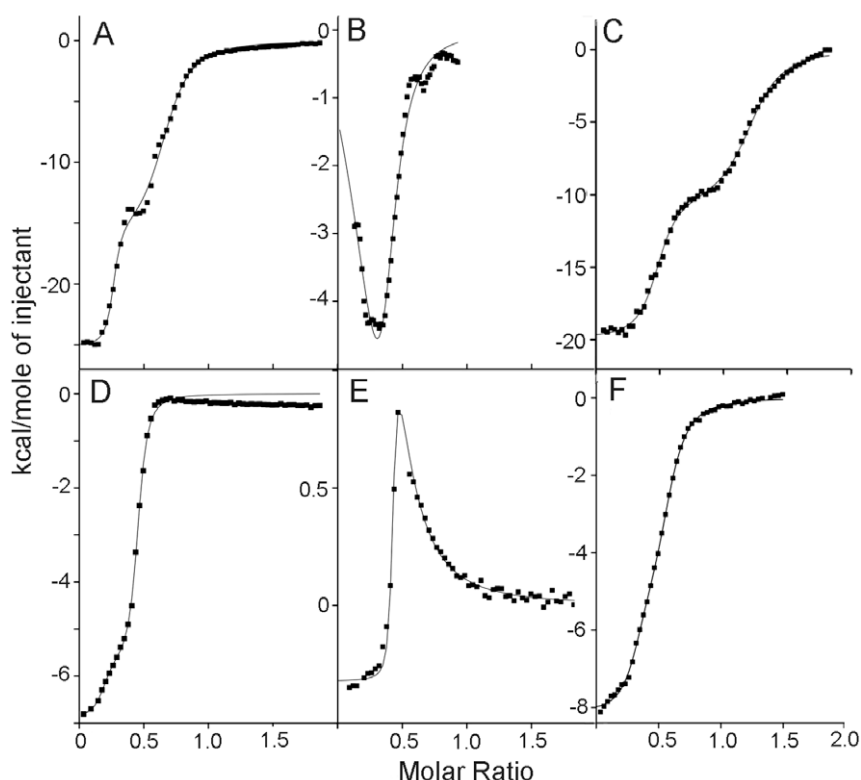
Fig. 10. Binding isotherm of 3.2 mM HgCl$_2$ (A), HAuCl$_4$ (B), AgNO$_3$ (C), NiCl$_2$ (D), ZnCl$_2$ (E), or FeCl$_3$ (F) into 400 μM mb (cell) aqueous solution at 25 °C. Binding isotherm of 1.6 mM HAuCl$_4$ (B). The curve fittings for two-site binding algorithm were used.

mobilization and transport of radionuclides and heavy metals from these sites to surrounding areas [33–39]. Methanotrophic bacteria are often present at these sites and often used in the remediation of halogenated hydrocarbons [40]. The results presented in this report indicate they may also be responsible or involved in the mobilization of radionuclides and heavy metals. For example, studies by Jenkins et al. [18] showed that soluble extracellular extracts produced by methanotrophs increased the transport of Cd(II) in porous soil columns. On the other hand, the reduction of several group A metals can also result in the metal immobilization.

The mechanism of metal binding by non-Cu group A metals showed a number of similarities originally observed with Cu group. First, at low metal concentrations, mb appeared to bind non-Cu Group A metals as a tetramer or oligomer via THI and HTI. Second, all of Group A metals tested were reduced by mb. Third, at metal to mb ratios between 0.25 and 0.5 metal per mb, the metals are coordinated via a mb dimer followed by a monomer at equimolar metal to mb concentrations. Fourth, at least in the case of Au, more than one metal atom was reduced per mb. Taken together the results suggest non-Cu group A metals followed a metal binding and reduction scheme similar to copper for all group A metals (Fig. 1). However, the CD-spectra suggest the final conformation changes associated with non-Cu group A metals differed from that observed following copper binding.

The results presented here also suggest the mechanism of binding to group B metals differ from that observed with group A metals [8]. Mb appears to bind group B metals as a tetramer or dimer depending on the metal concentration via THI (Fig. 1). With respect to the mechanism of binding, group B metals appear to follow the initial binding steps observed with group A metals which also initially binds copper via THI (Fig. 1) [8].

4. Abbreviations

ΔA	absorption change
CD	circular dichroism
CT	charge transfer
Ag–mb	methanobactin silver complex
Ag–mb	methanobactin gold complex
Cd–mb	methanobactin cadmium complex
Co–mb	methanobactin cobalt complex
Cu–mb	methanobactin copper complex
Fe–mb	methanobactin iron complex
Hg–mb	methanobactin mercury complex
Mn–mg	methanobactin manganese complex
Ni–mb	methanobactin nickel complex
Pb–mb	methanobactin lead complex
U–mb	methanobactin uranium complex
Zn–mb	methanobactin zinc complex
EPR	electron paramagnetic resonance
HTI	4-hydroxy-5-thiocarbonyl imidazolate

ITC	isothermal titration calorimetry
K	binding constant
Mb	methanobactin
MMO	methane monooxygenase
PMMO	membrane-associated methane monooxygenase
SMMO	soluble methane monooxygenase
THI	4-thiocarbonyl-5-hydroxy imidazolate
TEM	transmission electron microscopy
XPS	X-ray photoelectron spectroscopy

Acknowledgements

References

[1] A.A. DiSpirito, R.C. Kunz, D.W. Choi, J.A. Zahn, in: D. Zannoni (Ed.), Respiration in Archaea and Bacteria, Kluwer Scientific, The Netherlands, 2004, pp. 141–169.

[2] A.A. DiSpirito, J.A. Zahn, D.W. Graham, H.J. Kim, C.K. Larive, T.S. Derrick, C.D. Cox, A. Taylor, J. Bacteriol. 180 (1998) 3606–3616.

[3] H.J. Kim, D.W. Graham, A.A. DiSpirito, M. Alterman, N. Galeva, D. Asunskis, P. Sherwood, C.K. Larive, Science 305 (2004) 1612–1615.

[4] C.M. Tellez, K.P. Gaus, D.W. Graham, R.G. Arnold, R.Z. Guzman, Appl. Environ. Microbiol. 64 (1998) 1115–1122.

[5] J.A. Zahn, A.A. DiSpirito, J. Bacteriol. 178 (1996) 1018–1029.

[6] D.-W. Choi, W.A. Antholine, Y.S. Do, J.D. Semrau, C.J. Kisting, R.C. Kunz, D. Campbell, V. Rao, S.C. Hartsel, A.A. DiSpirito, Microbiology 151 (2005) 3417–3426.

[7] D.-W. Choi, R.C. Kunz, E.S. Boyd, J.D. Semrau, W.E. Antholine, J.-I. Han, J.A. Zahn, J.M. Boyd, A.M. de la Mora, A.A. DiSpirito, J. Bacteriol. 185 (2003) 5755–5764.

[8] D.-W. Choi, C.J. Zea, Y.S. Do, J.D. Semrau, W.E. Antholine, M.S. Hargrove, N.L. Pohl, E.S. Boyd, G.G. Geesey, S.C. Hartsel, P.H. Shafe, M.T. McEllistrem, C.J. Kisting, D. Campbell, V. Rao, A.M. de la Mora, A.A. DiSpirito, Biochemistry 45 (2006) 1442–1453.

[9] M.W. Fitch, D.W. Graham, R.G. Arnold, S.K. Agarwal, P. Phelps, G.E.J. Speitel, G. Georgiou, Appl. Environ. Microbiol. 59 (1993) 2771–2776.

[10] H.J. Kim, N. Galeva, C.K. Larive, M. Alterman, D.W. Graham, Biochemistry 44 (2005) 5140–5148.

[11] J.D. Morton, K.F. Hayes, J.D. Semrau, Environ. Sci. Technol. 34 (2000) 4917–4922.

[12] P.A. Phelps, G.E. Agarwal, G.E.J. Speitel, G. Georgiou, Appl. Environ. Microbiol. 58 (1992) 3701–3708.

[13] V. Braum, H. Killmann, Trends Biochem. Sci. 24 (1999) 104–109.

[14] J.H. Crosa, C.T. Walsh, Microbiol. Mol. Biol. Rev. 66 (2002) 223–249.

[15] M. Di Lorenzo, S. Poppelaars, M. Stork, M. Nagasawa, M.E. Tolmasky, J.H. Crosa, J. Bacteriol. 186 (2004) 7327–7336.

[16] J. Neilands, B., J. Biol. Chem. 270 (1995) 26723–26726.

[17] H.-H. Nguyen, S.J. Elliott, J.H.-K. Yip, S.I. Chan, J. Biol. Chem. 273 (1998) 7957–7966.

[18] M.B. Jenkins, J.-H. Chen, D.J. Kadner, L.W. Loin, Appl. Environ. Microbiol. 60 (1994) 3491–3498.

[19] J.P. Greenstein, M. WinitzChemistry of the Amino Acids, vol. 2, John Wiley & Sons Inc., New York, 1961.

[20] M.-Y. Chae, A.W. Czarnik, J. Am. Chem. Soc. 114 (1992) 9704–9705.

[21] A.W. CzarnikFluorescent Chemosensors for Ion and Molecule Recognition, vol. 538, American Chemical Society, Washington, DC, 1992.

[22] S. Barazzouk, P.V. Kamat, S. Hotchandani, J. Phys. Chem. B 109 (2005) 716–723.

[23] G.D. Fasman, Circular Dichroism and the Conformational Analysis of Biomolecules, Plenum Press, New York, 1996.

[24] N. Berova, K. Nakanishi, R.W. Woody, Circular Dichroism; Principles and Applications, second ed., Wiley VCH, New York, 2000.

[25] P. Crews, J. Marcel, R. Jaime, Organic Structure Analysis, Oxford University Press, New York, 1998.

[26] B.F. Matzanke, G. Muller-Matzanke, K.N. Raymond, in: T.M. Loehr (Ed.), Iron Carriers and Iron Proteins, VCH Publishers, Inc., New York, 1989.

[27] C.D. Bain, A. Biebuyck, G.M. Whitesides, Langmuir 5 (1989) 725–727.

[28] J. Riga, J.J. Verbist, J. Chem. Soc. Perkin Trans. II (1983) 1545–1553.

[29] C.D. Wagner, A.V. Naumkin, A. Kraut-Vass, J.W. Allison, C.J. Powell, J.R.J. Rumble, US Nat. Inst. Stand. Technol. (2005).

[30] P. Demange, A. Bateman, A. Dell, M.A. Abdallah, Biochemistry 27 (1988).

[31] P. Demange, A. Bateman, C. Mertz, A. Dell, Y. Piemont, M.A. Abdallah, Biochemistry 29 (1990) 11041–11051.

[32] J.B. Neilands, Adv. Inorg. Biochem. 5 (1983) 138–166.

[33] R.T. Anderson, H.A. Vrionis, I. Ortiz-Bernad, C.T. Resch, P.E. Long, R. Dayvault, K. Karp, S. Marutzky, D.R. Metzler, A. Peacock, D.C. White, M. Lowe, D.R. Lovley, Appl. Environ. Microbiol. 69 (2003) 5884–5891.

[34] H.L. Ehrlich, Appl. Microbiol. Biotechnol. 48 (1993) 687–692.

[35] L.R. Krumholz, D.A. Elias, J.M. Suflita, Geomicrobiol. J. 20 (2003) 61–72.

[36] J.G. Lack, S.K. Chaudhuri, S.D. Kellly, K.M. Kemner, S.M. O'Connor, J.D. Coates, Appl. Environ. Microbiol. 68 (2002) 2704–2710.

[37] N. Matsumoto, Y. Motoda, T. Matsuo, T. Nakashima, N. Re, F. Dahan, J.-P. Tuschague, Inorg. Chem. 38 (1999) 1165–1173.

[38] N. Parmer, L.A. Warren, E.E. Roden, F.G. Ferris, Chem. Geol. 169 (2000) 281–288.

[39] Y. Suzuki, S.D. Kelly, K.M. Kemner, J.F. Banfield, Appl. Environ. Microbiol. 71 (2005) 1790–1797.

[40] R.L. Hanson, T.E. Hanson, Microbiol. Rev. 60 (1996) 439–471.